Visible-Light-Driven BiOBr-TiO2-Attapulgite Photocatalyst with Excellent Photocatalytic Activity for Multiple Xanthates

Yaozhong Qi , Sikai Zhao * , Xiaoyu Jiang , Zhangke Kang , Shuling Gao , Wengang Liu , Yanbai Shen *

Posted Date: 16 November 2023

doi: 10.20944/preprints202311.1110.v1

Keywords: BiOBr-TiO2-attapulgite; ternary composites; photocatalysis; visible light; xanthates.

Article

Visible-Light-Driven BiOBr-TiO_2-Attapulgite Photocatalyst with Excellent Photocatalytic Activity for Multiple Xanthates

Yaozhong Qi, Sikai Zhao *, Xiaoyu Jiang, Zhangke Kang, Shuling Gao, Wengang Liu and Yanbai Shen *

School of Resources and Civil Engineering, Northeastern University, Shenyang 110819, China
* Correspondence: zhaosikai@mail.neu.edu.cn (S.Z.); shenyanbai@mail.neu.edu.cn (Y.S.)

Abstract: The novel ternary composites, BiOBr-TiO_2-attapulgite (BTA), were synthesized using a simple hydrothermal and water-bath method, exhibiting excellent photocatalytic performance to multiple xanthates. For BTA photocatalyst, TiO_2 and BiOBr were uniformly loaded on the surface of acid-activated attapulgite. As a widely used collector in mining processes, sodium ethyl-xanthate (SEX) was selected as the target pollutant due to its high toxicity. The BTA ternary photocatalyst demonstrated significantly higher adsorption and photocatalytic degradation performance compared to TiO_2 nanoparticles, BiOBr nanosheets, and BiOBr-TiO_2 heterojunction. Structural characterization and experimental results indicated that the exceptional photocatalytic degradation efficiency of BTA was mainly attributed to the formation of heterojunction between BiOBr and TiO_2, as well as the presence of additional active adsorption sites provided by attapulgite. Free radical scavenging experiments and EPR results confirmed that the photogenerated holes were the predominant active species to photodegrade SEX throughout the entire experiment. The LC-MS results provided insight into potential degradation pathways of SEX. This research demonstrates that BTA, as a novel triple composite material, achieves rapid and complete degradation to 20 mg/L SEX within 20 min. This work presents a novel approach to synthesize mineral-based photocatalysts, which have broad prospects for application in flotation wastewater treatment.

Keywords: BiOBr-TiO_2-attapulgite; ternary composites; photocatalysis; visible light; xanthates

1. Introduction

With the advancement of mining operations, flotation has become an indispensable process in ore dressing, resulting in the production of a significant volume of flotation wastewater that has the potential to contaminate the natural environment [1,2]. Xanthate, due to its cost-effectiveness and outstanding flotation capabilities, has been emerged as a crucial collector for sulfide minerals and gold ores [3]. Although a substantial amount of xanthate is consumed during the flotation process, there is still a considerable presence of xanthate in the wastewater, ranging from 5 to 40 mg/L [4]. Such high concentration of xanthate brings a severe threat to both the environment and human health, which should be paid enough attention to eliminate its harmful effects [5]. Xanthate-containing wastewater has a detrimental impact on aquatic ecosystems, primarily due to its rich organic and chemical composition, which exhibits toxic effects on aquatic organisms [6]. It also poses a serious threat to the local economy and food security of the region. Furthermore, xanthate-containing wastewater presents potential risks to human health, damaging nervous and digestive systems and inducing cancer. Especially, the decomposition of xanthate will generate CS_2 gas, which irreversibly damages the respiratory system [7,8]. In order to highly reduce the hazards released by xanthate-containing wastewater, some proactive and effective measures should be implemented.

Photocatalysis, as one of the advanced oxidation processes (AOPs), is popular owing to its high efficiency, environmental friendliness, and sustainability [9]. Up to now, the extensive research of photocatalytic degradation technology for the treatment of xanthate-containing wastewater has been carried out to mitigate pollution [10]. The utilization of light energy for catalyzing the degradation of

 doi:10.20944/preprints202311.1110.v1

xanthate-containing wastewater enables the achievement of water management and purification objectives [10,11].

Titanium dioxide (TiO_2) is a commonly employed semiconductor material in photocatalysis, renowned for its responsiveness to ultraviolet light, stability, cost-effectiveness, and environmental friendliness [12]. Nonetheless, the photocatalytic performance of single TiO_2 (T) faces some limitations, such as wide bandgap, low response to visible light, rapid recombination of e^-/h^+ pairs and agglomeration by high surface energy [13]. To tackle these challenges, employing suitable carriers and creating heterostructures with other semiconductors are effective strategies to restrain the recombination of electron-hole pairs, which can increase visible light utilization efficiency, prevent TiO_2 agglomeration, and ultimately enhance photocatalytic efficiency under visible light [14,15].

Coupling TiO_2 on the surface of a carrier can effectively improve the dispersibility of TiO_2 [16,17]. So far, significant attention has been given to employing clay minerals as a catalytic substrate to reduce production costs and disperse catalysts [18]. Attapulgite (A) is a layered silicate mineral with a nanoporous structure, which can effectively inhibit particle aggregation and increase active sites [17,19]. Due to its chemical inertness, resistance to deterioration, and cost-effectiveness for large-scale commercialization, attapulgite is widely used in various industrial, catalytic, and environmental applications [20]. Therefore, attapulgite-supported TiO_2 can form composite catalysts with a large number of active sites, raising the contact frequency between the catalyst and pollutants, and thus enhancing photocatalytic activity [20–22].

To address the wide bandgap of TiO_2 (~3.0 eV), the formation of heterojunction can further effectively reduce the bandgap width, prevent the recombination of electron-hole pairs, and thus generate more active species for enhancing the photocatalytic activity [23]. Due to its narrower bandgap compared with TiO_2, BiOBr (B) can absorb visible light and enhance the visible light activity of photocatalyst. As a typical two-dimensional semiconductor material, BiOBr exhibits excellent crystallinity, forming highly crystalline nanosheets that maintain their integrity throughout the photocatalytic process [24,25]. Additionally, it has been observed that tight coupling heterojunctions through chemical bonding can establish efficient charge transfer pathways, thus greatly reduce photo-induced carrier recombination [26]. The construction of a BiOBr/TiO_2 (BT) type II heterojunction, with TiO_2 acting as the primary catalyst and BiOBr as the co-catalyst, can prolong the transfer distance and separation time of e^-/h^+ pairs, enable the utilization of the visible light spectrum and considerably enhance the efficiency of visible light utilization [27–29].

The BiOBr-TiO_2-attapulgite (BTA) composites were synthesized through hydrothermal and water-bath method in this study. Xanthates were selected as the target pollutants because they are highly toxic and their release into ecosystems poses a severe threat to human health and significant environmental problems. The application parameters of the photocatalyst were investigated to determine the optimal conditions for xanthate degradation. The characterization results and experimental data were used to propose potential photocatalytic degradation pathways and mechanisms.

2. Results and discussion

2.1. Characterization of materials

2.1.1. Phase analysis

X-ray diffraction (XRD) analysis can determine the crystalline structure of materials by identifying their corresponding diffraction peaks. In Figure 1(a), it can be seen that the diffraction peaks located at 25.28°, 36.95°, and 48.05° are well matched with the crystal planes (101), (103), and (200) of anatase TiO_2 (JCPDS No. 21-1272) [30]. The XRD patterns also exhibit peaks at 10.90°, 21.93°, and 31.69°, which correspond to the crystal planes (001), (002), and (102) of BiOBr (JCPDS No. 09-0393) [31]. Besides, the presence of attapulgite (JCPDS No. 00-021-0550) is confirmed by the peaks at 13.90°, 19.85°, 26.7°, and 35.32°, which can be attributed to its crystal planes [32,33]. Furthermore, the

Preprints (www.preprints.org) | NOT PEER-REVIEWED | Posted: 16 November 2023 doi:10.20944/preprints202311.1110.v1

distinct peaks observed at 10.90° and 31.69° in the BT composites (Figure 1(b)) are in good agreement with the crystal planes of BiOBr, while the remaining diffraction peaks are consistent with the crystal planes of anatase TiO_2. Compared to BT, the diffraction peaks of BTA remain largely unchanged, with weak peaks observed at 26.7° and 35.32°. This suggests that the attapulgite has not a significant impact on the interaction between BiOBr and TiO_2. Moreover, the presence of these two additional weak peaks indicates the successful loading of BiOBr and TiO_2 onto attapulgite.

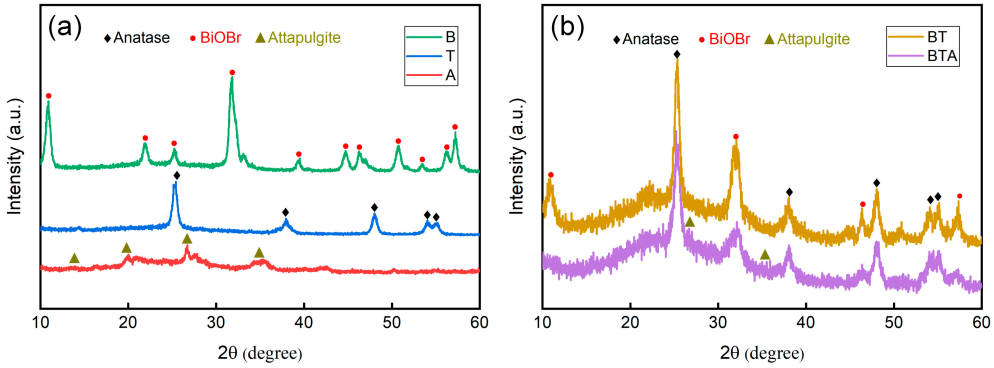

Figure 1. XRD patterns of (a) B, T, A and (b) BT, BTA samples.

2.1.2. Phase analysis

The morphology, microstructure and element distribution of samples are observed through scanning electron microscopy (SEM), transmission electron microscopy (TEM) and energy dispersive spectrum (EDS) analysis. Figures 2(a-b) show severe aggregation of nanostructured TiO_2 and BiOBr particles, which can be attributed to their high surface energy. Individual TiO_2 particle shows approximately 20~25 nm in size (Figure 2(a)). BiOBr is a representative two-dimensional material with dimensions ranging from approximately 200 to 400 nm in length and 6 nm in thickness (Figure 2(b)). The attapulgite presents a distinctive layered chain with fibrous aggregation morphology, facilitating the assembly of TiO_2 and BiOBr (Figure 2(c)). In Figure 2(d), BiOBr firmly adheres to the surface of TiO_2 to form BT binary composites, which can promote electron transfer through an increased contact area and thus improve catalytic reaction efficiency. Figure 2(e) demonstrates that the dispersion of TiO_2 and BiOBr in the BTA ternary heterogeneous system is notably improved when attapulgite is employed as a carrier. Combined with BET results (Table S1), the incorporation of attapulgite markedly enhances the specific surface area of BT composites, exceeding the dispersion achieved by BT binary materials. BTA effectively weakens the aggregation of BiOBr and TiO_2, resulting in the formation of ternary composites characterized by intimate contact and prominently exposed edges. This expands the contact area of photocatalysts with the target degradation substance and thus greatly enhances photocatalytic activity. Figure 2(f) presents a TEM image of BTA, exhibiting a close combination of attapulgite, TiO_2, and BiOBr, which is in good agreement with the SEM image. In the HRTEM image (Figure 2(g)), the lattice fringe spacings of BiOBr and TiO_2 are determined to be approximately 0.19 and 0.35 nm, corresponding to the (201) and (101) crystal planes of BiOBr and anatase TiO_2, respectively [3,34]. Element mappings (Figure 2(h)) and EDS analysis (Figure S2) identify the primary elements in BTA as Bi, O, Br, Ti, and Si. All these elements are uniformly distributed in composites, and the results confirm the coexistence of BiOBr, TiO_2, and attapulgite. The analysis further verifies the even distribution of TiO_2 nanoparticles and BiOBr nanosheets on the surface of attapulgite.

Preprints (www.preprints.org) | NOT PEER-REVIEWED | Posted: 16 November 2023 doi:10.20944/preprints202311.1110.v1

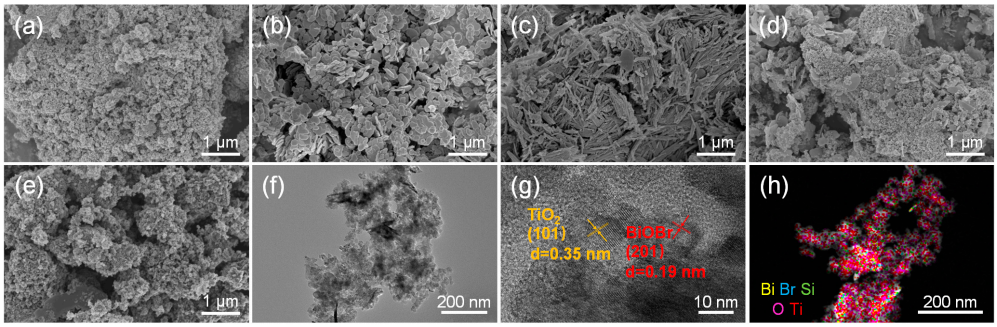

Figure 2. SEM images of (a) T, (b) B, (c) A, (d) BT, and (e) BTA. (f) TEM image, (g) HRTEM image, and (h) Element mappings of BTA composites.

2.1.3. Surface chemical state analysis

Figure 3 illustrates the elemental composition and binding states of BTA ternary composites using XPS analysis.

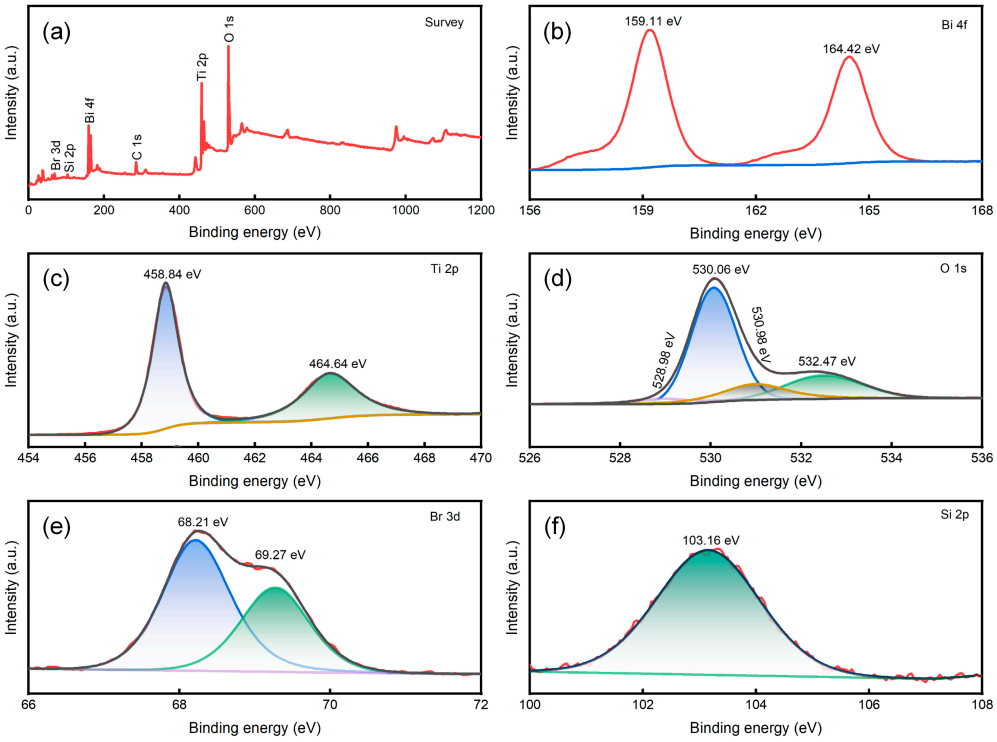

Figure 3. XPS spectra of BTA composites. (a) Survey scan; (b) Bi 4f; (c) Ti 2p; (d) O 1s; (e) Br 3d; (f) Si 2p.

Based on the complete spectrum displayed in Figure 3(a), the BTA ternary composites predominantly consist of five elements, namely Bi, Br, O, Ti, and Si. The peaks positioned at 159.11 and 163.42 eV in Figure 3(b) correspond to Bi $4f_{7/2}$ and Bi $4f_{5/2}$, respectively, indicating the presence of characteristic peaks associated with Bi^{3+} in BiOBr [35]. In Figure 3(c), the XPS spectra of Ti 2p exhibit peaks at 458.84 and 464.64 eV, which correspond to the normal state of Ti^{4+} in TiO_2 [36]. The XPS spectrum of O 1s is presented in Figure 3(d), revealing the presence of O in four distinct binding modes. The four peaks at 528.98, 530.06, 530.98, and 532.47 eV represent $[Bi_2O_2]^{2+}$, Ti-O, surface -OH groups, and Si-O, respectively [3]. In Figure 3(e), two peaks are observed at 68.21 and 69.27 eV, corresponding to Br $3d_{5/2}$ and Br $3d_{3/2}$, respectively, suggesting the presence of Br^{-1} in BiOBr [37]. Figure 3(f) exhibits the Si 2p spectrum, in which 103.16 eV corresponding to the presence of SiO_2 in

Preprints (www.preprints.org) | NOT PEER-REVIEWED | Posted: 16 November 2023 doi:10.20944/preprints202311.1110.v1

attapulgite [38]. The XPS results provide additional evidence for the strong incorporation of BiOBr and TiO_2 into the attapulgite carrier, indicating a more comprehensive integration rather than mere mixing.

2.1.4. TG-DSC analysis

Thermogravimetric and differential scanning calorimetry (TG-DSC) curves in Figure 4 are used to describe the mass change of BTA composites with increasing temperature [39,40]. Evaporation, phase transition, and chemical reactions are the primary factors contributing to the decrease in sample mass. Below 270.3°C, the 3.94% decrease in mass of BTA composites is primarily attributed to the loss of water adsorbed on its surface. With a further increase in temperature up to 477.6°C, there is an approximate 1.29% in mass loss, resulting from the evaporation of structural water in attapulgite. The increase in progressive temperature leads to an approximately 11.27% in mass loss with an exothermic process, signifying the formation of new substances. Herein, this process is likely to involve the decomposition of BiOBr under high temperature condition, yielding $Bi_{24}O_{31}Br_{10}$ and Br_2 gas, resulting in heat release and mass loss [41]. The analysis of TG-DSC curves highlights the significance of selecting an optimal calcination temperature to achieve a good photocatalytic performance in BTA ternary materials.

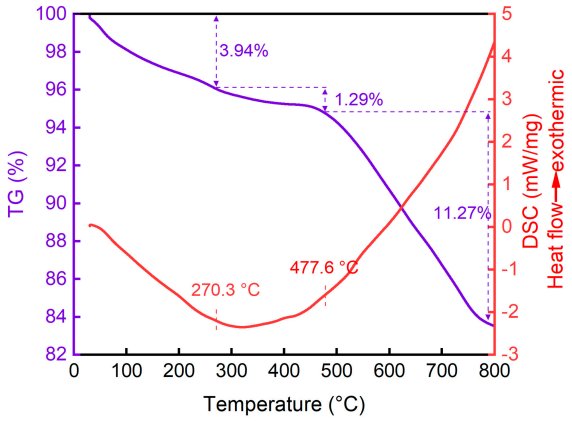

Figure 4. TG-DSC curves of BTA composites.

2.2. Photocatalytic activity

Figure 5 compares the degradation efficiency curves and kinetic curves of different samples of TiO_2, BiOBr, BT, and BTA to SEX, aiming to demonstrate the robust photocatalytic performance of BTA. The experiment employed a visible light intensity of 400 W, an SEX initial concentration of 20 mg/L, and a catalyst dosage of 0.2 g/L. Based on Figure 5(a), the adsorption of SEX by photocatalysts reaches dynamic equilibrium within 30 min of the dark reaction. Compared to the other samples, BTA ternary composites exhibit significantly enhanced adsorption performance to SEX. This improvement can be ascribed to the addition of attapulgite weakens the aggregation of TiO_2 and BiOBr, significantly increasing the availability of active sites for SEX attachment. In contrast, TiO_2 demonstrates negligible photodegradation efficiency to SEX under visible light, indicating limited utilization of visible light and capability to degrade SEX. While BiOBr and BT exhibit more pronounced degradation performance to SEX, and BT demonstrates higher degradation efficiency compared to BiOBr. This observation suggests that the formation of heterogeneous structures between TiO_2 and BiOBr can effectively improve the overall photocatalytic performance. BTA ternary composites exhibit a remarkable enhancement in photocatalytic degradation efficiency, with a first-order reaction rate constant of 0.11699 min^{-1}, which is approximately 3.1 times higher than that of BT. Such finding suggests that the generation of more active sites on the surface of BTA composites

Preprints (www.preprints.org) | NOT PEER-REVIEWED | Posted: 16 November 2023 doi:10.20944/preprints202311.1110.v1

promotes not only increased adsorption of SEX molecules but also rapid progress in the photocatalytic degradation reaction.

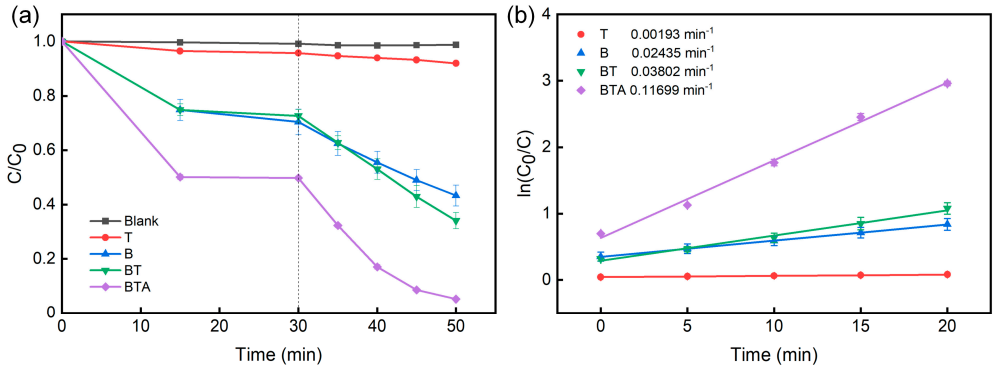

Figure 5. (a) Degradation efficiency curves and (b) kinetic curves of different samples to 20 mg/L SEX.

To effectively serve future industrial applications, it is imperative to carefully select suitable conditions and parameters for photocatalytic applications. The applicability of BTA composites was thoroughly evaluated by examining the dosage of photocatalysts, concentration of xanthate, applicable pH range of wastewater, feasibility of degradation of various xanthates, and stability of photocatalysts.

Figures 6(a-b) illustrate the degradation efficiency curves and kinetic curves of BTA composites with different dosages to 20 mg/L SEX. In the experiment, a 50 mL solution of SEX was served as the reaction medium. The dosage of BTA composites was the only variable, systematically set at 0.10, 0.15, 0.20, 0.25, and 0.30 g/L. With the increase of photocatalyst dosage, the adsorption performance gradually increases and reaches adsorption-desorption dynamic equilibrium within 30 min. Over the course of the photocatalytic stage, the degradation effect of SEX intensifies with time, while the photocatalytic rate initially increases and subsequently decreases with increasing photocatalyst dosage. As the dosage of the photocatalyst is raised from 0.10 to 0.20 g/L, the degradation rate of SEX increases due to the augmented number of catalytic sites in the ternary materials. Nonetheless, when the photocatalyst dosage further increases from 0.20 to 0.30 g/L, the catalytic rate begins to decelerate, possibly as a result of the excessive BTA photocatalyst obstructing visible light and diminishing its intensity. Consequently, for the treatment of xanthate-containing wastewater with a concentration of 20 mg/L, the BTA dosage ranging from 0.15 to 0.30 g/L can attain a photocatalytic degradation efficiency exceeding 90%. Obviously, the BTA dosage of 0.20 g/L exhibits the highest reaction rate in the degradation of SEX. Hence, such photocatalyst dosage is selected as the optimal condition for subsequent optimization.

The concentration of xanthate in discharged wastewater is typically around 10–30 mg/L [4]. Therefore, in this section, simulative mineral wastewater with xanthate concentration of 10–30 mg/L was used for the investigation, and the corresponding results of photocatalytic degradation of BTA composites are presented in Figures 6(c-d). As the SEX concentration increases from 10 to 25 mg/L, the photocatalyst exhibits a decreasing trend in adsorption performance and the first-order reaction kinetic constant representing the photocatalytic performance. However, it is worth noting that when the SEX concentration increases to 30 mg/L, there is a slight enhancement observed in the adsorption performance of BTA composites. The main reason for this phenomenon is that, under the condition of keeping the active adsorption sites of BTA unchanged, the excess of SEX molecules enhances the likelihood of attaching to the surface of BTA composites. Within the SEX concentration ranging from 10 to 30 mg/L, all of the degradation efficiencies are around 90%, indicating that 0.20 g/L of BTA demonstrates outstanding degradation performance in practical applications. With increasing SEX concentration, the rate of photocatalytic degradation initially increases and subsequently decreases. The fastest photocatalytic degradation rate, achieving a degradation efficiency of 94.8%, is observed

Preprints (www.preprints.org) | NOT PEER-REVIEWED | Posted: 16 November 2023 doi:10.20944/preprints202311.1110.v1

at SEX concentration of 20 mg/L. Taking into account the subsequent experimental conditions, 20 mg/L of xanthate is chosen as the optimal condition to achieve the best degradation rate of SEX.

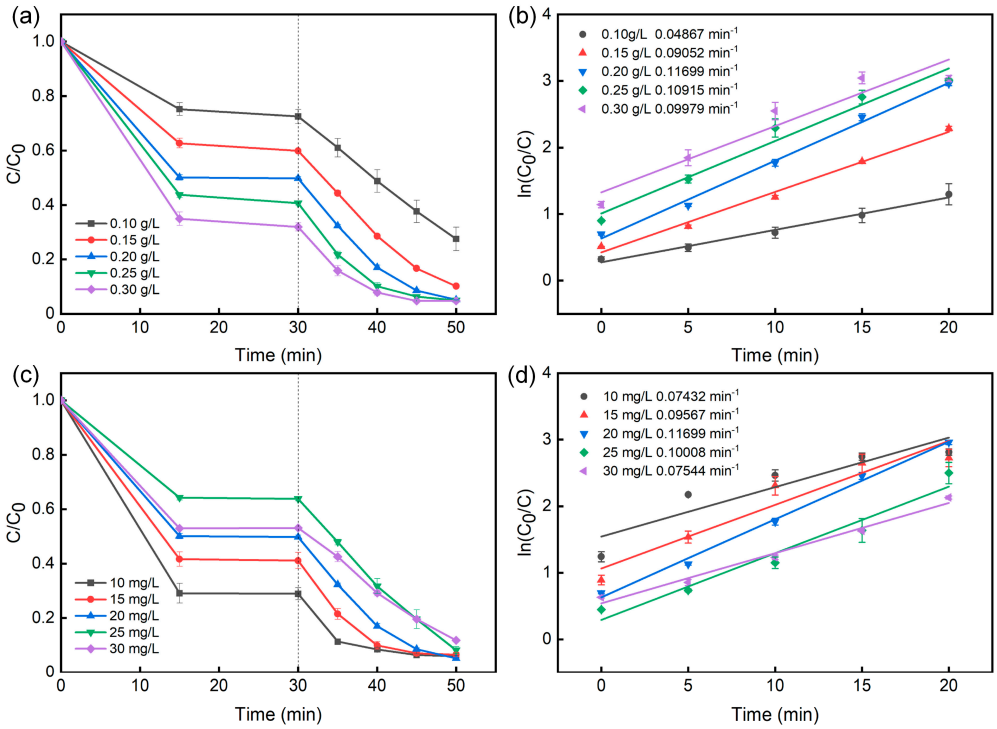

Figure 6. (a) Degradation efficiency curves and (b) kinetic curves of BTA composites with different dosages to 20 mg/L SEX. (c) Degradation efficiency curves and (d) kinetic curves of 0.20 g/L BTA composites to various initial concentrations of SEX.

It is widely acknowledged that pH plays a crucial role in determining the surface charge of photocatalysts and the composition of pollutants, thereby exerting a profound influence on their photodegradation efficiency. Figure 7 demonstrates the degradation performance of 20 mg/L SEX under different pH conditions with and without 0.20 g/L of BTA composites. With the pH changes from 5 to 11, the minimal SEX self-decomposition occurs in the wastewater system without photocatalysts. However, when BTA composites are introduced, an impressive degradation efficiency of approximately 90% is achieved within a narrower pH ranging from 5 to 9 (around 7.45 without any pH adjustment). Nevertheless, it should be noted that once pH value exceeds 11, the catalytic activity towards wastewater degradation by this photocatalyst diminishes significantly. This phenomenon could potentially arise from either a decline in active oxygen groups generated by BTA composites under alkaline conditions. Consequently, in practical wastewater treatment processes, BTA composites could rapidly and effectively degrade SEX molecules within a pH range of 5 to 9.

Preprints (www.preprints.org) | NOT PEER-REVIEWED | Posted: 16 November 2023 doi:10.20944/preprints202311.1110.v1

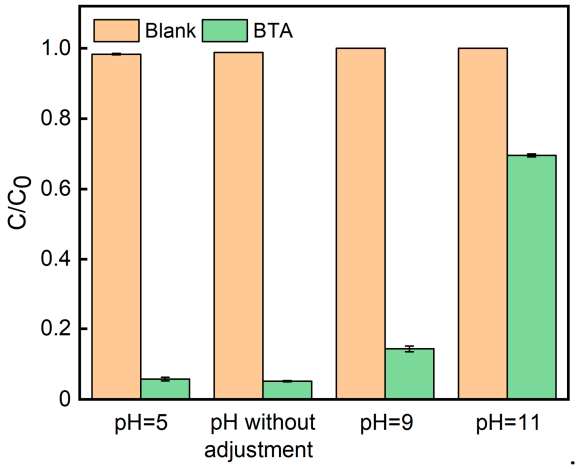

Figure 7. Degradation efficiency of 20 mg/L SEX at different pH values with and without 0.20 g/L of BTA composites.

Due to the widespread mixed usage of different types of xanthates in mining plants, Figure 8 illustrates the degradation efficiencies of various xanthates with a concentration of 20 mg/L under visible light conditions using 0.20 g/L of BTA composites. The adsorption capacity of BTA composites for different types of xanthates is correlated with the length of their side chains. This phenomenon can be attributed to the fact that longer-chain xanthate molecules exhibit stronger adhesion characteristic because of their relatively complex spatial structure, thus increasing their likelihood of adhering to the surface sites of BTA composites. 20 min later, the degradation rates of SEX, SBX, SIPX, and SIAX reach 94.8%, 95.2%, 89.4%, and 97.3%, respectively. Therefore, it can be inferred that BTA composites universally degrade xanthates, confirming compatibility of BTA with complex xanthate compositions in mining wastewater.

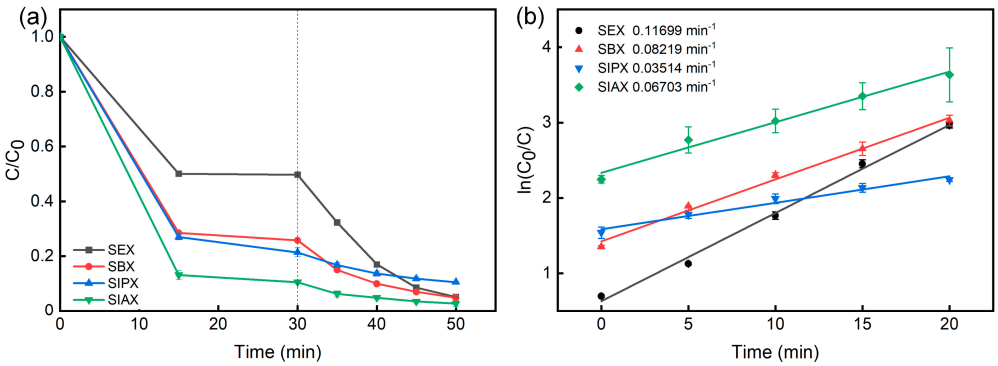

Figure 8. (a) Degradation efficiency curves and (b) kinetic curves of 0.20 g/L BTA composites with different types of xanthates.

In practical applications, the stability of photocatalysts is of great importance. Figure 9 demonstrates the microstructure changes of the BTA ternary photocatalyst by presenting XRD patterns and SEM images before and after the photocatalytic degradation process, along with an assessment of its long-term stability and reusability. From the XRD patterns shown in Figure 9(a), it is found that BTA composites exhibit minimal changes before and after the reaction, indicating that the catalytic process does not disrupt the original lattice parameters. SEM images in Figures 9(b-c) clearly illustrate that the post-reaction BTA composites maintain a distinct outline, in which TiO_2 nanoparticles are visibly presented, while BiOBr nanosheets remain supporter on TiO_2. Consequently, the morphology of attapulgite is not revealed due to encapsulation by TiO_2. This

Preprints (www.preprints.org) | NOT PEER-REVIEWED | Posted: 16 November 2023 doi:10.20944/preprints202311.1110.v1

implies that the morphology of BTA composites does not undergo significant alterations. In the long-term stability test, as shown in Figure 9(d), the freshly prepared composites exhibit a photocatalytic degradation efficiency of 94.9%. Over a 30-day period, the degradation efficiency shows no significant change and remains above 90%, suggesting that BTA composites are suitable for long-term storage and practical applications. Additionally, Figure 9(e) illustrates the reusability of the BTA photocatalyst. A single photocatalytic process involves 30 min of dark adsorption followed by 20 min of photocatalytic reaction. As the number of cycles increases, the adsorption of SEX molecules by BTA composites decreases. The possible reason is that a small quantity of SEX molecules and intermediate products persist on the surface of the BTA photocatalyst after the completion of the reaction, and thus reducing the adsorption sites of photocatalyst. After three cycles, the degradation rate of xanthate by BTA composites still exceeds 90%, showing that the excellent degradation efficiency is maintained. This observation highlights the ability of the multi-photocatalytic process to maintain the structure and heterojunction of BTA without disruption. Overall, it provides a valuable guideline for the long-term stability and efficient recycling ability of BTA photocatalysts in practical applications.

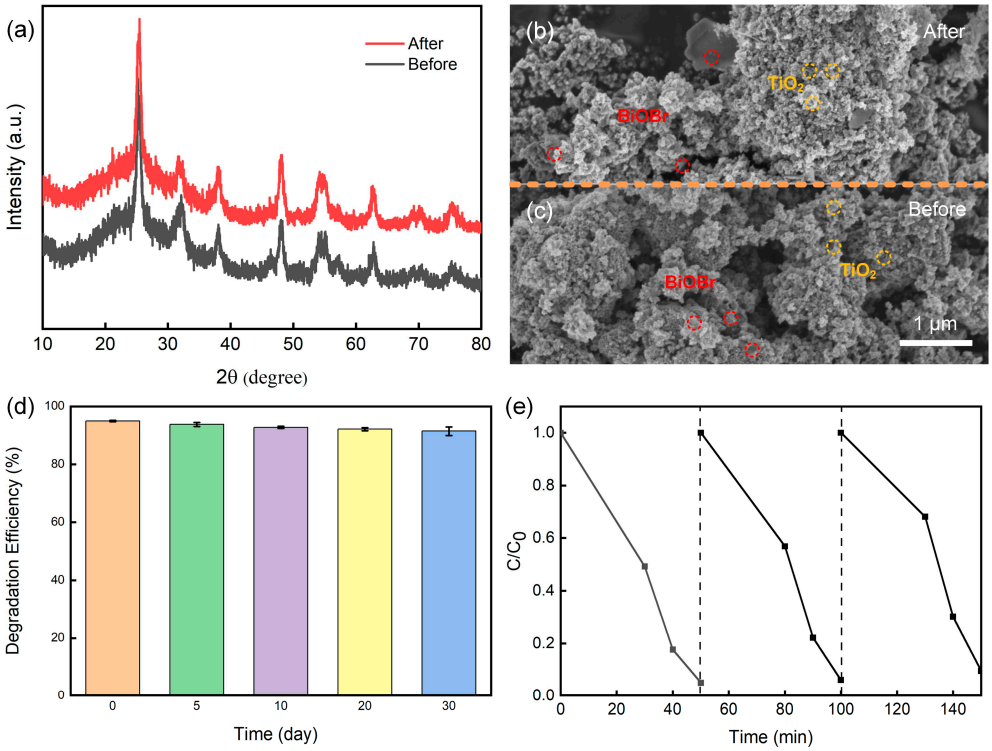

Figure 9. (a) XRD patterns and (b-c) SEM images of BTA composites before and after photocatalytic degradation reaction. (d) Long-term stability and (e) recycling performance of BTA composites.

2.3. Possible degradation mechanism

In order to further explore the possible photodegradation pathway of SEX molecules, liquid chromatography-mass spectrometry (LC-MS) was used to analyze the content of simulated wastewater after photocatalysis for 5 min, and the results are shown in Figure S3. Based on the value of m/z, four possible intermediates are assumed: $CH_3O_2S_2^-$ (m/z=112.1), $C_2H_5O_2S_2^-$ (m/z=126.2), $C_2H_5O_2S_2^-$ (m/z=141.1) and $C_4H_5OS_4^-$ (m/z=198.1&199.1). The specific chemical structures of the intermediates are presented in Table S2. By analyzing real-time absorbance changes, conducting free radical activity tests, and examining the LC-MS results, the potential degradation pathways of SEX are provided in Figure 10. The BTA photocatalyst generates a significant number of photogenerated holes, thereby leading to the strong oxidation of SEX molecules to $CH_3O_2S_2^-$, $C_2H_5O_2S_2^-$, $C_2H_5O_2S_2^-$, and

Preprints (www.preprints.org) | NOT PEER-REVIEWED | Posted: 16 November 2023 doi:10.20944/preprints202311.1110.v1

$C_4H_5OS_4^-$ etc. It indicates that SEX and the intermediate products are eventually decomposed into smaller inorganic molecules, including CO_2, H_2O, and SO_4^{2-}, through continuous oxidation by free radicals.

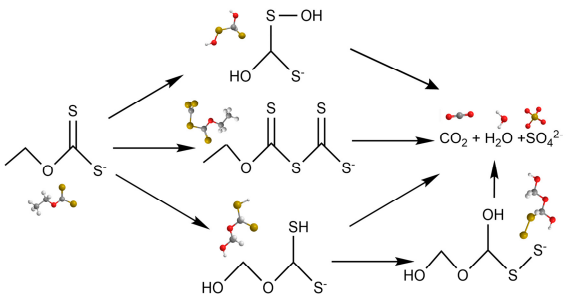

Figure 10. Possible degradation pathway of SEX.

To investigate the synergistic degradation effect of xanthate by different free radicals, a free radical trapping experiment was conducted. $AgNO_3$, p-benzoquinone (BQ), isopropyl alcohol (IPA) and EDTA-2Na, are selected to trap e^-, ·OH, $\cdot O_2^-$ and h^+ radicals, respectively. As shown in Figure 11(a), the addition of EDTA-2Na leads to a significant decrease in degradation efficiency of SEX, reducing it to 7.9%. BQ addition also exhibits a certain effect with a reduction in degradation efficiency by 19.1%. However, the presence of IPA and $AgNO_3$ solution minimally impact the catalytic efficiency. These experiments highlight the dominant role of h^+ radicals as active species in the oxidative decomposition of xanthate molecules. In order to elucidate the predominant role of photogenerated holes in the reaction process and the mechanism of electron-hole pair separation, TEMPO is employed for qualitative detection of h^+ production as shown in Figure 11(b). TEMPO exhibits a 1:1:1 signal in analysis and possesses stable chemical properties. The TEMPO molecules combine with the holes to form TEMPOH, which weakens the EPR response, leading to attenuation of the EPR peak. Thus, the reduction in EPR signal intensity is an indicator for holes generation. Under dark conditions, a more pronounced characteristic peak corresponding to TEMPO-h^+ is observed; whereas under visible light irradiation, a diminished characteristic signal peak indicates participation and consumption of photogenerated holes. This observation confirms the crucial involvement of photogenerated holes in the overall photocatalytic reaction.

During the experiment, real-time absorption spectra of the simulated wastewater containing SEX were measured at various time intervals in order to demonstrate the degradation process of SEX by BTA composites (Figure 11(c)). Initially, two absorption peaks are clearly observed at 226 and 301 nm, respectively, corresponding to the absorption peak of SEX. After 20-min period of photocatalytic degradation, the intensity of both peaks decreases, indicating the gradual decomposition and disappearance of SEX during the reaction. As the reaction progressing further, no new absorption peak emerges in the simulated wastewater from mineral processing, and the original peak intensity diminishes. This suggests that both SEX and its intermediate products are broken down into smaller molecules over time.

The absorption peak strength of PL was utilized to characterize the recombination rate of electron-hole pairs. As depicted in Figure 11(d), the absorption peak intensity of PL for BTA composites exhibits a tendency to decrease in comparison to BT. This observation suggests that the presence of attapulgite in conjunction with BT leads to a further reduction in the recombination rate of electron-hole pairs. Consequently, a larger number of photogenerated electrons and holes are available to engage in the degradation reaction of xanthate, consequently enhancing the rate of photocatalytic degradation.

Preprints (www.preprints.org) | NOT PEER-REVIEWED | Posted: 16 November 2023 doi:10.20944/preprints202311.1110.v1

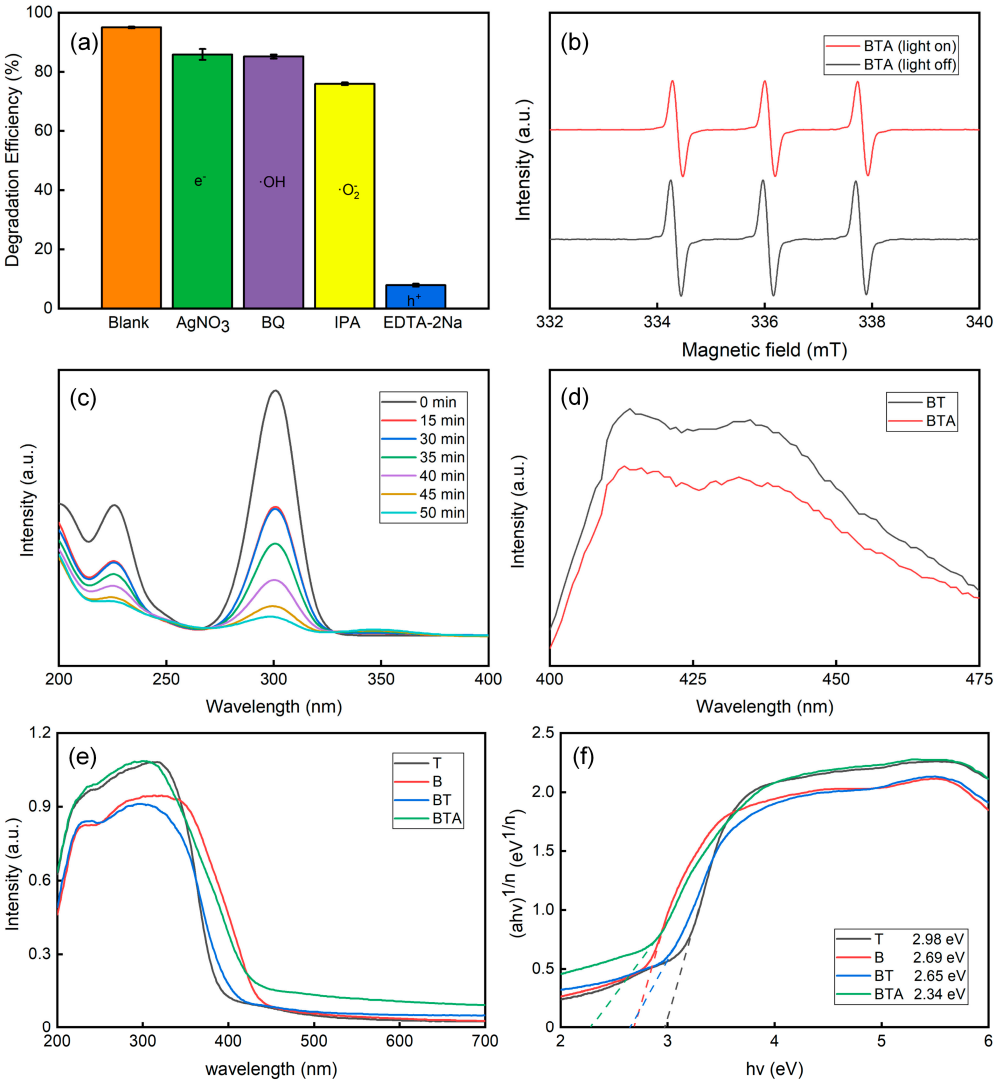

Figure 11. (a) Effect of scavenger on the degradation efficiency of SEX. (b) EPR spectra of TEMPO-h+. (c) Real-time curves of absorbance change of SEX. (d) PL spectra. (e) UV–vis DRS and (f) Band gaps of different samples.

The photochemical capacity and bandgap energy (E_g) of the as-prepared samples were determined using UV-vis DRS. As shown in Figures 11(e-f), it reveals that TiO_2 and BiOBr exhibit absorption edges at 396 and 435 nm, respectively. When the photocatalyst is combined with attapulgite carrier, the optical absorption band edge of BTA composites undergoes a redshift towards longer wavelengths, indicating that the obtained ternary materials significantly enhance their response to visible light, thereby improving photocatalytic activity. The bandgap widths of different materials were calculated using the Tauc-Plot method, as shown in Figure 11(f). The bandgap widths for T, B, BT, and BTA are determined to be 2.98, 2.69, 2.65, and 2.34 eV respectively. BT has a narrower bandgap width compared to TiO_2 and BiOBr due to the generation of a heterojunction. Furthermore, upon loading BT onto attapulgite carrier, BTA exhibits a further decrease in its bandgap to 2.34 eV, implying that the formed composites promote electron-hole pair separation, leading to increased generation of radical and accelerated degradation reaction rates under visible light irradiation conditions. The valence band potentials (E_{VB}) of TiO_2 and BiOBr are 2.69 and 3.12 eV, respectively [3,42]. Combined with the bandgap width of the material and the formula of $E_{CB} = E_{VB} - E_g$, the conduction band potentials (E_{CB}) for TiO_2 and BiOBr can be estimated to be -0.29 and 0.43 eV, respectively.

Preprints (www.preprints.org) | NOT PEER-REVIEWED | Posted: 16 November 2023 doi:10.20944/preprints202311.1110.v1

Based on the microstructural characterization and the photodegradation performance efficiency of the photocatalyst, the corresponding improvement in BTA's ability to harness visible light can be attributed to heterojunction formation and dispersion of attapulgite carrier. The enhancement of photocatalytic performance can be attributed to three main reasons: (1) Attapulgite, acting as a carrier, effectively alleviates the agglomeration of TiO_2 and BiOBr and reduces grain size. (2) Attapulgite provides more active adsorption sites and photocatalytic reaction sites for BTA composites, thereby improving the adsorption and catalytic performance of SEX molecules on photocatalysts. (3) The construction of a "type II" heterojunction increases the separation time of photogenerated electron-hole pairs by extending the transport distance of photogenerated carriers, thereby enhancing the photocatalytic reaction activity.

Figure 12 illustrates the degradation mechanism of SEX molecules on the surface of BTA ternary photocatalyst. After the introduction of attapulgite, SEX is more likely to attach to the reactive active site of BTA composites. Under visible light irradiation, the photogenerated electrons of TiO_2 conduction band (CB) migrate to the CB of BiOBr due to the lower reduction point of TiO_2. Simultaneously, the photogenerated holes produced by the valence band (VB) in BiOBr transfer to the VB of TiO_2. The migration of photogenerated carriers effectively prevents the recombination of electron-hole pairs, leading to prolonged contact time with SEX molecules and improved photocatalytic efficiency. SEX molecules are initially decomposed into $CH_3O_2S_2^-$, $C_2H_5O_2S_2^-$, $C_2H_5O_2S_2^-$ and $C_4H_5OS_4^-$ under the action of ROS groups dominated by h^+ and supplemented by e^-, ·OH, and $\cdot O_2^-$. Over time, these intermediate products further are decomposed into smaller compounds until they are converted into CO_2, H_2O, SO_4^{2-}, etc.

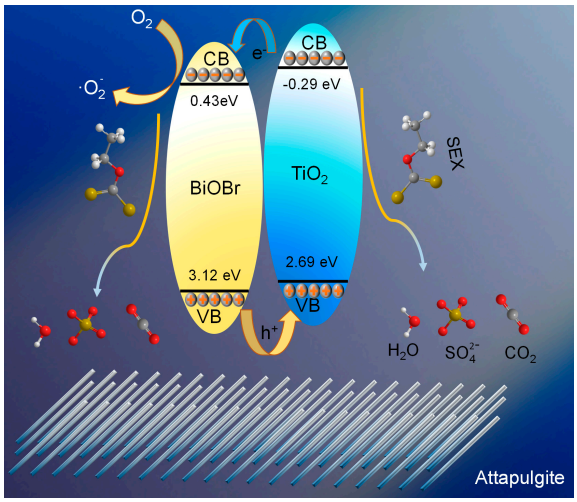

Figure 12. Possible degradation mechanism of SEX under visible light by BTA composites.

3. Materials and Methods

The detail description for materials, microstructure characterization methods, composites synthesis route and measurement procedure of photocatalytic activity can be found in Supporting Text I.

4. Conclusions

BTA ternary composite photocatalyst was synthesized using a two-step method involving hydrothermal and water-bath routes. Within BTA composites, TiO_2 and BiOBr were uniformly grown, distributed, and coated onto the surface of acid-treated attapulgite, displaying excellent dispersibility and binding properties. The synthesized BTA composites exhibited highly efficient degradation of SEX molecules under visible light conditions within 20 min. The remarkable degradation efficiency of BTA composites could be attributed to the abundant active adsorption and photocatalytic reaction sites provided by attapulgite, as well as the formation of heterojunctions

between BiOBr and TiO_2. Through the mechanism of primarily photogenerated holes, the SEX molecules could be converted into CO_2, H_2O, and SO_4^{2-} via possible degradation pathways. BTA composites offer the advantages of low production cost, the ability to degrade various xanthates, and excellence recycling performance, thereby demonstrating its potential for treating flotation wastewater. The optimal BTA composites presents an efficient, low-energy consumption, and cost-effective solution for flotation wastewater treatment.

Supplementary Materials: The following supporting information can be downloaded at the website of this paper posted on Preprints.org. Figure S1. Absorbance standard curve of SEX solution; Figure S2. EDS spectra of BTA composites; Figure S3. LC-MS pattern of SEX after a 5-min photocatalytic reaction; Table. S1 BET specific surface area of different composites; Table. S2 Chemical structures and m/z values of possible degradation intermediates of SEX.

Author Contributions: Y.Q.: Conceptualization, Methodology, Investigation, Validation, Visualization, and Writing—original draft. S.Z.: Conceptualization, Methodology, Investigation, Validation, and Funding acquisition. X.J. and Z.K.: Conceptualization and Methodology. S.G. and W.L.: Conceptualization, Methodology, and Supervision. Y.S.: Methodology, Writing—review, Resources, Supervision, and Funding acquisition. All authors have read and agreed to the published version of the manuscript.

Funding: The project was supported by the National Natural Science Foundation of China (52274255, 51674067), National Key R&D Program of China (2020YFB2008702), Fundamental Research Funds for the Central Universities (N2301003, N2201008, N2201004, N2301025), Liaoning Revitalization Talents Program (XLYC1807160), Postdoctoral Foundation of Northeastern University, Young Elite Scientists Sponsorship Program by CAST (2022QNRC001), and China Postdoctoral Science Foundation (2022M720025).

Data Availability Statement: The data presented in this study are available on request from the corresponding author.

Acknowledgments: Special thanks are due to the instrument and data analysis from Analytica and Test Center, Northeastern University.

Conflicts of Interest: The authors declare that they have no known competing financial interest or personal relationships that could have appeared to influence the work reported in this paper.

References

1. Shu, K.; Chuaicham, C.; Noguchi, Y.; Xu, L.; Sasaki, K., In-situ hydrothermal synthesis of Fe-doped hydroxyapatite photocatalyst derived from converter slag toward xanthate photodegradation and Cr(VI) reduction under visible-light irradiation. *Chemical Engineering Journal* **2023,** *459*, 141474.
2. Shen, M.; Zhang, G.; Liu, J.; Liu, Y.; Zhai, J.; Zhang, H.; Yu, H., Visible-light-driven photodegradation of xanthate in a continuous fixed-bed photoreactor: Experimental study and modeling. *Chemical Engineering Journal* **2023,** *461*, 141833.
3. Zhou, P.; Shen, Y.; Zhao, S.; Li, G.; Cui, B.; Wei, D.; Shen, Y., Synthesis of clinoptilolite-supported BiOCl/TiO_2 heterojunction nanocomposites with highly-enhanced photocatalytic activity for the complete degradation of xanthates under visible light. *Chemical Engineering Journal* **2021,** *407*, 126697.
4. Tan, Y.; Chen, T.; Zheng, S.; Sun, Z.; Li, C., Adsorptive and photocatalytic behaviour of PANI/TiO_2/metakaolin composites for the removal of xanthate from aqueous solution. *Minerals Engineering* **2021,** *171*, 107129.
5. Jia, Y.; Zhang, Y.; Zhang, X.; Cheng, J.; Xie, Y.; Zhang, Y.; Yin, X.; Song, F.; Cui, H., Novel CdS/PANI/MWCNTs photocatalysts for photocatalytic degradation of xanthate in wastewater. *Separation and Purification Technology* **2023,** *309*, 123022.
6. Shen, Y.; Zhou, P.; Zhao, S.; Li, A.; Chen, Y.; Bai, J.; Han, C.; Wei, D.; Ao, Y., Synthesis of high-efficient TiO_2/clinoptilolite photocatalyst for complete degradation of xanthate. *Minerals Engineering* **2020,** *159*, 106640.
7. Fallahpour, M.; Poursalehi, R.; Yourdkhani, A., Highly efficient photocatalytic removal of concentrated PEX, PAX and SIPX xanthates collectors by an immobilized nanostructured g-C_3N_4/ZnO low power backlighted module. *Minerals Engineering* **2023,** *204*, 108416.
8. Yuan, F.; Zheng, Y.; Gao, D.; Wang, L.; Hu, X., Facile assembly and enhanced visible-light-driven photocatalytic activity of S-scheme BiOBr/g-C_3N_4 heterojunction for degrading xanthate in wastewater. *Journal of Molecular Liquids* **2022,** *366*, 120279.
9. Chen, X.; Wang, Z.; Shen, X.; Zhang, Y.; Lou, Y.; Pan, C.; Zhu, Y.; Xu, J., A plasmonic Z-scheme Ag@AgCl/PDI photocatalyst for the efficient elimination of organic pollutants, antibiotic resistant bacteria and antibiotic resistance genes. *Applied Catalysis B: Environmental* **2023,** *324*, 122220.

10. Zhou, P.; Shen, Y.; Zhao, S.; Chen, Y.; Gao, S.; Liu, W.; Wei, D., Hydrothermal synthesis of novel ternary hierarchical MoS_2/TiO_2/clinoptilolite nanocomposites with remarkably enhanced visible light response towards xanthates. *Applied Surface Science* **2021,** *542*, 148578.
11. Zhou, P.; Shen, Y.; Zhao, S.; Bai, J.; Han, C.; Liu, W.; Wei, D., Facile synthesis of clinoptilolite-supported Ag/TiO_2 nanocomposites for visible-light degradation of xanthates. *Journal of the Taiwan Institute of Chemical Engineers* **2021,** *122*, 231-240.
12. 12. Shu, K.; Chuaicham, C.; Noguchi, Y.; Xu, L.; Sasaki, K., Charge transfer mechanism through S-scheme heterojunction in in-situ synthesized TiO_2/Fe-doped hydroxyapatite for improved photodegradation of xanthate. *Jounral of Hazardous Materials* **2023,** *460*, 132337.
13. Li, G.; Teng, Q.; Sun, B.; Yang, Z.; Liu, S.; Zhu, X., Synthesis scaly Ag-TiO_2 loaded fly ash magnetic bead particles for treatment of xanthate wastewater. *Colloids and Surfaces A: Physicochemical and Engineering Aspects* **2021,** *624*, 126795.
14. Wang, C.; Zhang, B.; Zhao, Z.; Zhang, Z.; Zhang, S.; Bala, H.; Zhang, Z., Enhanced n-butanol sensing properties of Au modified TiO_2 nanorod arrays: A combined experimental and first-principle study. *Applied Surface Science* **2023,** *641*, 158458.
15. Bott-Neto, J. L.; Martins, T. S.; Oliveira Jr, O. N.; Marken, F., Controlled electrodeposition of brookite TiO_2 for photoelectroanalysis at printed carbon electrodes. *Applied Surface Science* **2023,** *640*, 158316.
16. Wang, S.-q.; Li, X.-x.; Wu, J.-j., Preparation of TiO_2/graphene oxide and their photocatalytic properties at room temperature. *Journal of Fuel Chemistry and Technology* **2022,** *50*, 1307-1316.
17. Meng, Z.; Wang, Y.; Liu, H.; Yan, Y.; Yan, F., Reinforced UHMWPE composites by grafting TiO_2 on ATP nanofibers for improving thermal and tribological properties. *Tribology International* **2022,** *172*, 107585.
18. Zhou, L.; Yan, Y.; Mao, H.; Zhou, S.; Hui, J.; Li, H.; Li, M.; Zhao, Y.; Zhang, Q.; Xia, S., Development of attapulgite based catalytic membrane for activation of peroxymonosulfate: A singlet oxygen-dominated catalytic oxidation process for sulfamethoxazole degradation. *Separation and Purification Technology* **2023,** *312*, 123382.
19. Yuan, S.; Peng, J.; Zhang, X.; Lin, D.; Geng, H.; Han, B.; Zhang, M.; Wang, H., A mechanically robust slippery surface with 'corn-like' structures fabricated by in-situ growth of TiO_2 on attapulgite. *Chemical Engineering Journal* **2021,** *415*, 128953.
20. Zhang, L.; Zhang, J.; Zhang, W.; Liu, J.; Zhong, H.; Zhao, Y., Photocatalytic activity of attapulgite–BiOCl–TiO_2 toward degradation of methyl orange under UV and visible light irradiation. *Materials Research Bulletin* **2015,** *66*, 109-114.
21. Tan, Z.; Zhang, S.; Yue, X.; Zhao, F.; Xi, F.; Yan, D.; Ling, H.; Zhang, R.; Tang, F.; You, K.; Luo, H. a.; Zhang, X., Attapulgite as a cost-effective catalyst for low-energy consumption amine-based CO_2 capture. *Separation and Purification Technology* **2022,** *298*, 121577.
22. Zhang, J.; Zhang, L.; Zhou, S.; Chen, H.; Zhong, H.; Zhao, Y.; Wang, X., Magnetically separable attapulgite–TiO_2–Fe O composites with superior activity towards photodegradation of methyl orange under visible light radiation. *Journal of Industrial and Engineering Chemistry* **2014,** *20*, 3884-3889.
23. Cao, W.; Wang, W.; Yang, Z.; Wang, W.; Chen, W.; Wu, K., Enhancing photocathodic protection performance by controlled synthesis of Bi/BiOBr/TiO_2 NTAs Z-scheme heterojunction films. *Journal of Alloys and Compounds* **2023,** *960*, 170675.
24. Yin, Y.; Kang, X.; Han, B., Two-dimensional materials: synthesis and applications in the electro-reduction of carbon dioxide. *Chemical Synthesis* **2022,** *2*, 19.
25. Liao, X.; Ren, H.-T.; Yang, T.; Shen, B.; Lin, J.-H.; Lou, C.-W.; Li, T.-T., A flexible, highly adaptive, self-standing photoelectrochemical aptasensor based on 3D pinecone-like structure BiOBr/TiO_2 hierarchical nanofiber membranes. *Ceramics International* **2023,** *49*, 27912-27921.
26. Mao, Y.; Wang, P.; Zhan, S., Shedding light on the role of interfacial chemical bond in heterojunction photocatalysis. *Nano Research* **2022,** *15*, 10158-10170.
27. Zhao, S.-Z.; Lu, Y.; Lu, R.; Hu, Y.-D.; Rodriguez, R. D.; Chen, J.-J., Constructing BiOBr/TiO_2 heterostructure nanotubes for enhanced adsorption/photocatalytic performance. *Journal of Water Process Engineering* **2023,** *54*, 103972.
28. 28. Eskandari, P.; Amarloo, E.; Zangeneh, H.; Rezakazemi, M.; Zamani, M. R.; Aminabhavi, T. M., Photocatalytic activity of visible-light-driven L-Proline-TiO_2/BiOBr nanostructured materials for dyes degradation: The role of generated reactive species. *Journal of Environmental Management* **2023,** *326*, 116691.
29. Li, G.; Shen, Y.; Zhao, S.; Bai, J.; Gao, S.; Liu, W.; Wei, D.; Meng, D.; San, X., Construction of rGO-SnO_2 heterojunction for enhanced hydrogen detection. *Applied Surface Science* **2022,** *585*, 152623.
30. Swathi, K. S.; Gopalakrishna Naik, K., Structural, morphological, and optical studies of sol–gel spin coated TiO_2 thin films. *Materials Today: Proceedings* **2023**, *960*, 170335.
31. Zhao, M.; Qin, J.; Wang, N.; Zhang, Y.; Cui, H., Reconstruction of surface oxygen vacancy for boosting CO_2 photoreduction mediated by BiOBr/CdS heterojunction. *Separation and Purification Technology* **2024,** *329*, 125179.

32. Li, B.; Li, L.; Zhang, Q.; Weng, W.; Wan, H., Attapulgite as natural catalyst for glucose isomerization to fructose in water. *Catalysis Communications* **2017,** *99*, 20-24.
33. Dong, L.; Wang, H.; Huang, Y.; Zha, J.; Cheng, H.; Liu, L.; Zhu, Z.; Chen, H.; Ding, S.; Wang, S., γ-Fe_2O_3 decorated attapulgite composite modified with $CuCl_2$ as magnetically separable sorbents for Hg0 removal from coal combustion flue gas. *Chemical Engineering Journal* **2021,** *408*, 127888.
34. Deng, J.; Xu, D.; Zhang, J.; Xu, Q.; Yang, Y.; Wei, Z.; Su, Z., $Cs_3Bi_2Br_9$/BiOBr S-scheme heterojunction for selective oxidation of benzylic C−H bonds. *Journal of Materials Science & Technology* **2023**, *924*, 166608.
35. Wu, M.; Zhang, B.; Wang, H.; Chen, Y.; Fan, M.; Dong, L.; Li, B.; Chen, G., Exposed 110 facets of BiOBr anchored to marigold-like $MnCo_2O_4$ with abundant interfacial electron transfer bridges and efficient activation of peroxymonosulfate. *Journal of Colloid and Interface Science* **2023,** *653*, 867-878.
36. Ma, J.; Zhang, L.; Fan, Z.; Sun, S.; Feng, Z.; Li, W.; Ding, H., Construction of R-TiO_2/n-TiO_2 heterophase photocatalysts for efficient degradation of organic pollutants. *Journal of Alloys and Compounds* **2023,** *968*, 172127.
37. Zhang, X.; Zhang, J.; Zha, X.; Luo, Y.; Hu, Y.; Chen, G.; He, X., Interfacial chemical bond and oxygen vacancies modulated Mo_2S_3/BiOBr high-low junctions for enhanced photocatalysis gatifloxacin degradation. *Applied Surface Science* **2023,** *641*, 158548.
38. Tan, Y.; Yin, C.; Zheng, S.; Di, Y.; Sun, Z.; Li, C., Design and controllable preparation of Bi_2MoO_6/attapulgite photocatalyst for the removal of tetracycline and formaldehyde. *Applied Clay Science* **2021,** *215*, 106319.
39. Liu, J.; Wang, B.; Liu, W.; Hu, X.; Zhang, C.; Zhou, Z.; Lang, J.; Wu, G.; Zhang, Y.; Yang, J.; Ni, Z.; Zhao, G., Regulating mechanical performance of poly (l-lactide acid) stent by the combined effects of heat and aqueous media. *International Journal of Biological Macromolecules* **2023,** *242*, 124987.
40. Wang, L.; Wang, T.; Zhang, Y.; Peng, X.; Song, W.; Yang, J.; Yuan, C., Oxidation behaviors of Hongqian heavy crude oil characterized by TG-DSC-FTIR-MS within full temperature regions. *Fuel* **2023,** *353*, 129242.
41. Zhu, S.-R.; Wu, M.-K.; Zhao, W.-N.; Yi, F.-Y.; Tao, K.; Han, L., Fabrication of heterostructured BiOBr/$Bi_{24}O_{31}Br_{10}$/TiO_2 photocatalyst by pyrolysis of MOF composite for dye degradation. *Journal of Solid State Chemistry* **2017,** *255*, 17-26.
42. Shi, Z.; Zhang, Y.; Shen, X.; Duoerkun, G.; Zhu, B.; Zhang, L.; Li, M.; Chen, Z., Fabrication of g-C_3N_4/BiOBr heterojunctions on carbon fibers as weaveable photocatalyst for degrading tetracycline hydrochloride under visible light. *Chemical Engineering Journal* **2020,** *386*, 124010.